

Isolating lithologic versus tectonic signals of river profiles to test orogenic models for the Eastern and Southeastern Carpathians

B. Gailleton^{1,3}, H. D. Sinclair¹, S. M. Mudd¹, E. L. S. Graf¹, L. Matenco²

¹University of Edinburgh, School of GeoSciences, Edinburgh, UK

²University of Utrecht, Department of Earth Sciences, Utrecht, The Netherlands

³Helmholtz Centre Potsdam, GFZ German Research Centre for Geosciences, Potsdam, Germany

Key Points:

- Misleading tectonic signals can be generated by lithologic contrasts
- Fluvial expression of tectonic activity can be obscured by more prominent forcings
- Tectonic forcing is successfully disentangled from lithology with systematic extraction of relative steepness index

Abstract

Fluvial morphology is affected by a wide range of forcing factors, which can be external, such as faulting and changes in climate, or internal, such as variations in rock hardness or degree of fracturing. It is a challenge to separate internal and external forcing factors when they are co-located or occur coevally. Failure to account for both factors leads to potential misinterpretations. For example, steepening of a channel network due to lithologic contrasts could be misinterpreted as a function of increased tectonic displacements. These misinterpretations are enhanced over large areas, where landscape properties needed to calculate channel steepness (*e.g.* channel concavity) can vary significantly in space. In this study, we investigate relative channel steepness over the Eastern Carpathians, where it has been proposed that active rock uplift in the Southeastern Carpathians gives way N- and NW-wards to ca. 8 Myrs of post-orogenic quiescence. We develop a technique to quantify relative channel steepness based on a wide range of concavities, and show that the main signal shows an increase in channel steepness from east to west across the range. Rock hardness measurements and geological studies suggest this difference is driven by lithology. When we isolate channel steepness by lithology to test for ongoing rock uplift along the range, we find steeper channels in the south of the study area compared to the same units in the North. This supports interpretations from longer timescale geological data that active rock uplift is fastest in the southern Southeastern Carpathians.

1 Introduction

Surface topography in upland landscapes and their surroundings is shaped by the competition between climatic and tectonic processes (*e.g.*, Beaumont et al., 1992; Avouac & Burov, 1996; Willett, 1999; Whipple, 2009). Tectonically induced surface motions can both build topography (*e.g.* mountain ranges by stacking tectonic units at convergent boundaries between plates) and create accommodation space in foreland basins that are filled with erosional products (*e.g.*, Sinclair, 2012). Surface processes, mainly driven by climatic forcings, will naturally tend towards equilibrating the mass surplus and deficits *via* erosion, transport and deposition of sediment (*e.g.*, D. et al., 1991; Allen, 2017; Tucker & van der Beek, 2013; Małenco et al., 2013). In theory, this competing system tends to make landscapes evolve towards a steady-state where surface motions are balanced by erosion and deposition (*e.g.*, Penck, 1953; J. T. Hack, 1960; Willett & Brandon, 2002). When perturbed, landscapes will move away from steady state forms, and geomorphologists have long been developing methods to unravel the occurrence, magnitude and timing of tectonic activity using the shape of the landscape (*e.g.*, A. A. C. de Lapparent, 1907; Tapponnier & Molnar, 1977; Arrowsmith et al., 1998; Zielke et al., 2010; Kirby & Whipple, 2012; Hurst et al., 2013; Mudd, 2017).

Studies aiming to link topography with tectonics have focused on the main erosive engine of non-glaciated landscapes: the river system (*e.g.*, J. T. Hack, 1960; Ahnert, 1970; Schoenbohm et al., 2004; Kirby & Whipple, 2012; Willett et al., 2014; Goren, 2016; Seagren & Schoenbohm, 2019). Amongst quantitative tools developed to describe fluvial morphology, channel steepness, or its normalised equivalent integrating discharge, has been perhaps most widely used. With the reasonable assumption that surface motions directly alter the gradient of channel networks, the contrasts in steepness have been interpreted as direct (steepening at fault contacts) or indirect (transient migration of steepening) signs of tectonic activity (*e.g.*, Kirby & Whipple, 2012). However, a variety of different forcings can affect channel steepness resulting in similar morphological expressions; lithology being a key factor. Where softer rocks give way downstream to harder rocks, a steadily eroding channel will steepen (*e.g.*, Forte et al., 2016; Perne et al., 2017; Yanites et al., 2017; Bernard et al., 2019). Critically, fault displacements commonly juxtapose different rock types, resulting in uncertainty about whether different channel steepnesses on either side of a fault are a function of different uplift rates, rock strength, or both. This common feature of geologically heterogeneous landscapes generates mixed signals in the river network, resulting in ambiguity in interpreting the main forcing controlling the steepening (*e.g.* Strong et al., 2019).

Here, we attempt to isolate the different forcings affecting channel steepness where both tectonic activity and lithology play a role. We focus on the Eastern and Southeastern Carpathians, where extracting the spatial distribution of active tectonic motions from river profiles is confounded by lithologic contrasts. We use a combination of (i) topographic analysis to extract channel steepness from Digital Elevation Models (DEMs) and (ii) field observations and measurements to constrain rock strength for the main lithologies. We then trace lithological units laterally from regions where active tectonics are thought to play a role, northward to where the range has been inactive for several millions of years. Through this exercise, we isolate the signal of active rock uplift on the river profiles from the role of lithology, and hence test tectonic models for the region.

2 Theoretical background

2.1 Fluvial geomorphometry

Scaling between channel steepness and discharge, or its proxy drainage area, has been qualitatively suggested and observed for over a century: “In general we may say that, if all else is equal, declivity bears an inverse relation to quantity of water” (p. 114 of Gilbert (1877)). In the mid-1950s, J. Hack (1957) and Morisawa (1962) quantified this qualitative observation, describing a systematic relationship between drainage area and channel gradient. These studies led to the formulation by Morisawa (1962) and later Flint (1974) of a power law describing the commonly observed decrease of channel gradient with increasing drainage area:

$$S = k_s A^{-\theta} \quad (1)$$

where S is the river gradient ($S = \frac{dz}{dx}$ where z is the elevation and x the distance along the channel); k_s the steepness index representing the overall gradient of a river system, a single river or one of its reaches; A the drainage area; and θ the concavity index dictating the rate at which channel gradient declines downstream. In order to compare different rivers over one or several networks, θ is commonly fixed to a reference value, frequently denoted θ_{ref} , in order to extract comparable steepness index values (*i.e.* normalised to the same value of the concavity index). k_s is then referred as k_{sn} , the normalised channel steepness.

Calculating k_s (or k_{sn}) and determining θ (or θ_{ref}) has been traditionally done by applying linear regressions of $\log(S) - \log(A)$ plots, where the gradient is $-\theta$ and the intercept k_s (e.g. Flint, 1974; C. Wobus et al., 2006; Kirby & Whipple, 2012). However, slope-area plots suffer from significant limitations, mainly linked to the inherently noisy nature of channel gradient derived from DEMs (e.g. Perron & Royden, 2013). It requires the use of averaging methods, inevitably resulting in data loss, to exploit the data (*e.g.* binning by drainage area and averaging the slope). An alternative method has been developed to mitigate the effects of topographic noise and binning of drainage area (L. H. Royden et al., 2000; Perron & Royden, 2013). This consists in integrating Eq.1 over the distance of the channel:

$$z(x) = z(x_b) + \left(\frac{k_s}{A_0^\theta}\right) \int_{x_b}^x \left(\frac{A_0}{A(x)}\right)^\theta dx \quad (2)$$

where x_b is the local base-level chosen for the analysis (*e.g.* a basin outlet or fixed elevation (Forte & Whipple, 2018)) and A_0 , a reference drainage area, which is introduced to non-dimensionalize drainage area. From this equation, L. H. Royden et al. (2000) defined a longitudinal coordinate χ as:

$$\chi = \int_{x_b}^x \left(\frac{A_0}{A(x)}\right)^\theta dx \quad (3)$$

Any point of the channel can be defined using χ such as:

$$z(x) = z(x_b) + \left(\frac{k_s}{A_0^\theta}\right)\chi \quad (4)$$

The χ approach normalises the river profile to a θ_{ref} and provides an alternative method to explore S-A relationships. If A_0 is set to a value of unity in Equation 3, then the gradient of χ -elevation is equal to k_s (e.g. Perron & Royden, 2013). χ has been widely used in various geomorphological studies linking channel morphology to surface processes, to investigate the evolution of drainage divides (e.g. Willett et al., 2014; Forte & Whipple, 2018; Giachetta & Willett, 2018; Seagren & Schoenbohm, 2019) or to derive topographic metrics to describe river networks (e.g. Hergarten et al., 2016; Wang et al., 2017; Gailleton et al., 2019).

2.2 Channel steepness, tectonics and lithology

k_s has been widely used as a proxy for geomorphological processes. Compilations of detrital cosmogenic nuclide concentrations (e.g. ^{10}Be), used to quantify average erosion rates for a given river catchment area (e.g. Lal, 1991; Bierman & Steig, 1996), have demonstrated a direct positive correlation between erosion rate and k_s (e.g. DiBiase et al., 2010; Kirby & Whipple, 2012; Scherler et al., 2014; Mandal et al., 2015; Harel et al., 2016; Codilean et al., 2018). This is a direct quantification of early hypotheses that steeper channels should tend to erode more rapidly (e.g. Gilbert, 1877; A. de Lapparent, 1896). Changes in erosion rates can result from tectonic or climatic forcings, enabling the use of k_s to study tectonic or climatic evolution over large areas.

In tectonically active landscapes, changes in k_s have been interpreted as a direct proxy for differential tectonic activity. C. W. Wobus, Whipple, & Hodges (2006) linked a sharp increase in channel steepness of the Marsyandi River as it crossed the region of the Main Central Thrust of the central Himalaya to a rock uplift signal related to the tectonic structure, using other proxies of erosion rates to support this hypothesis. This relationship between rock uplift and k_s has been thoroughly explored in a range of settings (e.g. Lavé & Avouac, 2001; C. Wobus et al., 2006; Seagren & Schoenbohm, 2019). Previous studies using both topographic data (e.g. Kirby & Whipple, 2012) and numerical models (e.g. Eizenhöfer et al., 2019) have highlighted potential explanations for large breaks in channel steepness. In both these studies, concentrated relative uplift could be caused by deep structures (e.g., midcrustal ramps) under the mountain belt. k_s has also been interpreted as an indirect expression of base-level change resulting from tectonics (e.g. C. Wobus et al., 2006; Ouimet et al., 2009; L. Royden & Perron, 2013; Steer et al., 2019; Hurst et al., 2019) or climate (B. T. Crosby & Whipple, 2006; Neely et al., 2017) driven, where steepened high k_s patches migrate upstream. Recent studies (e.g. Giachetta & Willett, 2018; Seagren & Schoenbohm, 2019) have also highlighted the effect of stream piracy on k_s , where captured areas disrupt the upstream drainage area and sediment supply balance, affecting the downstream channel steepness.

As tectonics, climate and stream piracy can affect channel steepness by inducing external forcings to the river channels, intrinsic forcings (e.g. fractures, weathering, lithology) will also affect k_s . Amongst these intrinsic forcings, the effect of differential lithology on fluvial morphology has been a recent focus of geomorphological studies (e.g. Kirby et al., 2003; Forte et al., 2016; Thaler & Covington, 2016; Yanites et al., 2017; Bezerra, 2018; Strong et al., 2019; Bernard et al., 2019; Seagren & Schoenbohm, 2019; Campforts et al., 2019). Rivers flowing over harder rocks tend to have steeper channels and affect the overall landscape morphology (e.g. Tucker & Slingerland, 1996; Forte et al., 2016; Yanites et al., 2017). This effect is linked to the sole fact that harder lithologies are more difficult to erode, forcing the channel to steepen to maintain a constant erosion rate. Studies of entire mountain ranges (e.g. Duvall, 2004; Bernard et al., 2019; Gabet, 2019) have demonstrated the important effect of lithology on channel steepness in syn- to post-orogenic settings, with

a positive correlation between k_{sn} and rock strength appearing to be the controlling forcing on landscape morphology in non-glaciated areas. Careful acknowledgement of lithological heterogeneities still permits the interpretation of climatic and tectonic signals from river morphology (e.g Kirby et al., 2003; Campforts et al., 2019), but can also confuse the signal (e.g. Strong et al., 2019) and potentially lead to misinterpretation. In this study, we focus on cases where contrasts in the erodibility of rock are co-located with contrasts in rock uplift. In that case, the origin of channel steepening remains difficult to interpret.

3 The orogenic and geomorphological evolution of the Eastern and South-eastern Carpathians

The Carpathians are an arcuate mountain range located in the eastern continuation of the Alpine orogenic belt (Fig. 1). Previous studies have shown that the overall Carpathian structure formed in response to the Triassic to Tertiary opening and closure of two oceanic realms by subduction and continental collision (details in Săndulescu, 1988; Csontos & Vörös, 2004; Maţenco, 2017; Schmid et al., 2019). In a plate tectonics scenario, the studied area of the Eastern and Southeastern Carpathians is made up by two basement-bearing continental mega-units in an upper plate position, the European (*sensu largo*) continental foreland in a lower plate position, and a thin-skinned thrust and fold belt deformed at or near their subduction contact (Figs. 1 and 2). The European foreland is furthermore overlain by a foredeep that locally reaches 13 km in the area of the Focşani Basin (Fig. 2, Tărăpoancă et al., 2003).

3.1 Tectonic evolution

The Middle Jurassic opening of the Alpine Tethys was followed by the Cretaceous-Miocene closure of its Pienides-Magura and Ceahlău-Severin branches (Fig. 1, Săndulescu, 1988; Schmid et al., 2008; Plašienka, 2018). The closure scraped off sediments deposited over the subducting ocean and its eastern passive continental margin by forming a thin-skinned system of thrust sheets, grouped in nappes emplaced in a foreland-breaking sequence from the Cretaceous (Ceahlău), late Oligocene to Early Miocene (Convolute Flysch, Audia/Macla), middle Miocene (Tarcau, Marginal Folds), to late middle Miocene to Early late Miocene (Subcarpathian) times (Figs. 1 and 2). The thin-skinned deformation took place until around 9-8 Ma when the main crustal subduction zone was locked by the continental collision (Schmid et al. 2008, Maţenco 2017 and references therein). Low temperature thermochronology studies, primarily apatite fission tracks and apatite U-Th/He, have shown that the thin-skinned accretion was associated with gradual exhumation. Exhumation of up to 6 km took place at average rates of below 1 mm/yr and peaked between 13 and 8 Ma during the Miocene collision (Sanders et al., 1999; Gröger et al., 2008; Merten et al., 2010; Necea, 2010). The exhumation was spatially distributed throughout the thin-skinned nappes with higher values in their centre (around the Tarcau and Marginal Folds nappes in Fig. 2). Similar exhumation rates were also interpreted in the northern part of the Eastern Carpathians during two periods of exhumation, one more rapid between 12 and 5 Ma and another after 5 Ma. In this area, the exhumation history is interpreted to be driven by the erosion of a thickened wedge after the cessation of shortening at 12-11 Ma, associated either with slab break-off or with the end of subduction (Andreucci et al., 2015).

While tectonic activity remained minor elsewhere, a further deformation episode took place after 8 Ma in the area of the Southeastern Carpathians. The formation of high-angle thick-skinned reverse faults truncating both the basement and the overlying thin-skinned thrust belt at depth created a crustal root presently located beneath the external parts of the thrust belt (Fig. 2), as proven by seismic, gravity and magnetic studies (e.g. Bocin et al., 2005, 2009; Hauser et al., 2007). This deformation was associated with gradually accelerating exhumation at values between 1.5 - 5 mm/yr in the external part of the orogenic wedge, located above the thick-skinned reverse faults (Merten et al., 2010; Necea, 2010). This

presently active deformation was also coeval with subsidence in the foreland at values of 1-3 mm/yr, which created the overall synclinal geometry of the Focșani Basin (Fig. 2, Tărăpoancă et al., 2003; K. A. Leever et al., 2006; Mațenco et al., 2007). It was also coeval with smaller amounts of subsidence in the order of hundreds of meters, creating the shallow Brașov and Tg. Secuiesc intramontane basins, which covered most of the internal part of the orogenic wedge and its Dacia basement (Fig. 1). These differential vertical motions are thought to be related to an asthenospheric circuit driven by the sinking Vrancea slab, still (barely) attached to the overlying lithosphere in the final stages of slab detachment (Martin & Wenzel, 2006; Ismail-Zadeh et al., 2012; Mațenco et al., 2016). The post-8 Ma tectonic structures of the Southeastern Carpathians, deformation along thick skinned reverse faults and the larger underlying mantle circuit, are presently active, as demonstrated by the large intermediate mantle (70 - 220 km) seismicity of the Vrancea slab, the moderate seismicity of the overlying crust (Oncescu & Bonjer, 1997; Radulian et al., 2000; Bocin et al., 2009; Ismail-Zadeh et al., 2012), and GPS movements reaching up to 7 mm/yr (van der Hoeven et al., 2005; Schmitt et al., 2007), together with interpretations from studies of the mantle structure, anisotropy and attenuation (Popa et al., 2005, 2008; Russo et al., 2005; Martin & Wenzel, 2006; Ivan, 2007; Bokelmann & Rodler, 2014).

3.2 Lithology and geomorphology

The Eastern and Southeastern Carpathians show a large diversity of mostly clastic, but also carbonatic lithologies across the orogenic strike, which maintains a remarkable continuity in the same tectonic units over hundreds of kilometers along its strike. The Cretaceous - Paleogene sedimentation is generally dominated by a deep-water mixture between pelagic and dominantly turbiditic (“flysch”) sedimentation, with shallower shelf to alluvial coarse sediments deposited in forearc basins over the accretionary wedge during peak tectonic moments (such as the Albian Ceahlău conglomerates), well described in numerous regional or local studies (e.g. Săndulescu, Ștefănescu, et al., 1981; Săndulescu, Krautner, et al., 1981; Melinte-Dobrinescu et al., 2008; Belayouni et al., 2009; Miclăuș et al., 2009; Olariu et al., 2014; Roban et al., 2017). A gradual transition towards a regressive basin fill (“molasse”) and coarser deposition took place during the Miocene continental collision in the more external Marginal Folds and Subcarpathian nappes, while the foredeep contains a middle Miocene - Pleistocene transition from shallow-water marine and lacustrine sedimentation dominated by an orbitally-forced cyclicity to a deltaic and alluvial continental sedimentation (e.g. Săndulescu, Ștefănescu, et al., 1981; Vasiliev et al., 2004; Jipa & Olariu, 2013; Stoica et al., 2013).

Geomorphological studies available in the Eastern and Southeastern Carpathians (Rădoane et al. 2017 and references therein) are in general agreement with the tectonic scenario described above. These studies have inferred that the Eastern Carpathians have a general topography that mirrors the decay of an older (Miocene) orogenic buildup, with longitudinal river profiles trending towards an equilibrium, and sediments generated dominantly by river channel erosion. In contrast, the Southeastern Carpathians have a young and actively changing topography, shown by a significant disequilibrium in longitudinal river profiles, sediments generated dominantly by recycling landslides, rapid uplift observed in geomorphic markers such as terraces, migration of knickpoints, water divides, and possible piracy events derived from χ profiles (see also Rădoane et al., 2003; Necea et al., 2005; K. Leever, 2007; Bălțeanu et al., 2010; ter Borgh, 2013; Cristea, 2014, 2015; Necea et al., 2013). These studies also suggested that recent tectonics may have shifted the presently observed main water divide separating rivers draining to the European foreland from those draining to the Transylvanian hinterland and the middle of the thin-skinned wedge in the central part of the Southeastern Carpathians (compare maps in Fig. 1). Furthermore, the tectonically induced differential vertical movements may have triggered a general drainage re-organization with rivers being deflected towards the center of the Focșani Basin (Fielitz & Seghedi 2005 and references therein). While all these indications point towards a differentiation in the Eastern and Southeastern Carpathians between the erosion of an older tectonic relief and

a topography controlled by active tectonics, respectively, the mechanisms responsible for the significant variability observed locally are less understood. For instance, structural and geomorphological studies have suggested that the Pleistocene to recent uplift of the Southeastern Carpathians has migrated eastwards through time towards the Focșani Basin (Fig. 2, Necea et al., 2005; Molin et al., 2012; Necea et al., 2013), qualitatively interpreted as an effect of the Vrancea slab steepening and retreating in the same direction (e.g. Mațenco et al., 2007). On this first order pattern, the locally observed influence of lithological strength contrasts on the surface morphology and heterogeneities in normalized channel steepness (Cristea, 2015; Rădoane et al., 2017) still has to be quantified.

In summary, all previous studies have suggested that the fluvial morphology is controlled by local and regional tectonics modulated by lithological variations. We build on these studies by applying our fluvial geomorphometry and channel steepness analysis at the scale of the entire Eastern and Southeastern Carpathians for rivers draining into the European hinterland. Furthermore, we explore the consistency of channel steepness variations across ranges of concavity indices constrained in the field area. We delimit the area into three regions controlled by different base levels (Fig. 1): (i) the Focșani Basin area, which aggregates rivers draining into the Southeastern Carpathians foreland basin, (ii) the Siret base level, aggregating rivers into the foreland basin along the entire chain, and (iii) the Prut base level and the associated drainage system, which is used as a reference area located far into the European foreland that is not directly linked with Carpathians mountain building processes. Our analysis specifically excludes the southern-most termination of the Southeastern Carpathians (the Ialomita catchment) with a Danube river base level (Fig. 1), as this is affected by significant strike-slip to transpressive deformation and recent salt diapirism (Mațenco & Bertotti, 2000). In the same area, our analysis also excludes the comparatively smaller internal part of the orogenic wedge that drains into the Transylvanian hinterland.

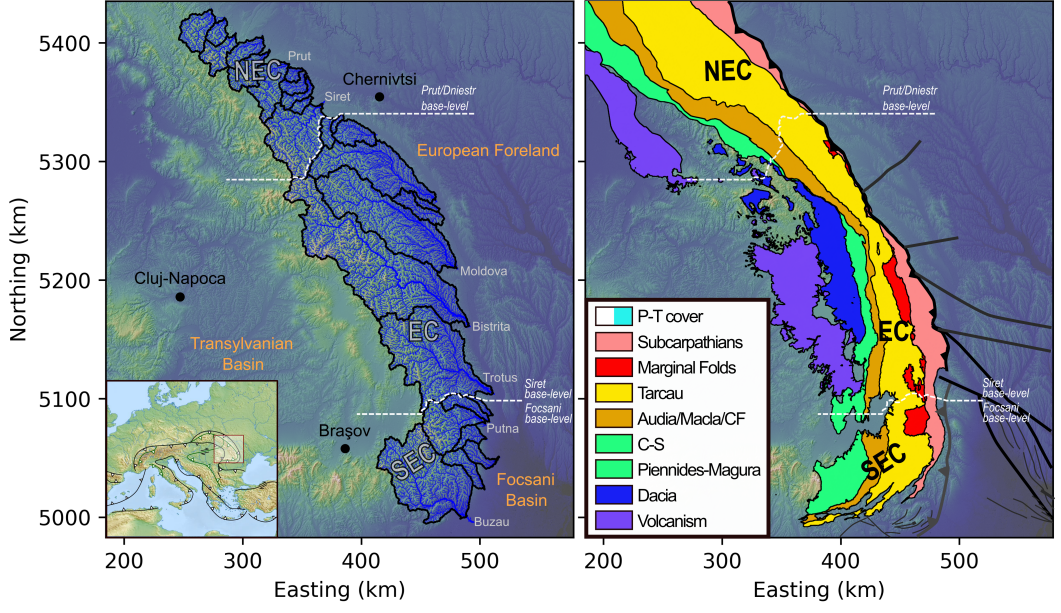


Figure 1. Location of the extracted channel network and the tectonic units in the Eastern and Southeastern Carpathians (Adapted from Andreucci et al. (2015); Maţenco (2017)). Note the different references used for Prut/Dniestr, Siret and Focşani base-levels. EC = Eastern Carpathians, SEC = South-Eastern Carpathians, NEC = North-Eastern Carpathians, P-T = Post-Tectonic cover (*sensu* post Late Miocene Collision), CF = Convolute Flysches and C-S = Ceahlău-Severin. Note the post-tectonic cover is not displayed on this figure for clarity purposes. The main frontal thrust is displayed in black where reaching the surface and grey where buried below the sediments of the Focşani basin.

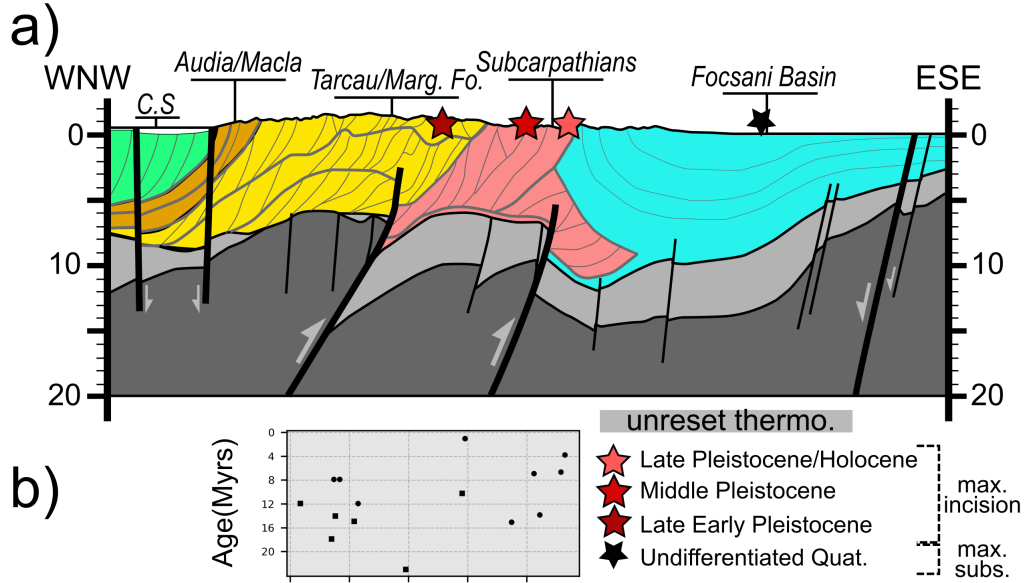


Figure 2. a) Sketch of simplified cross-section across the South-East Carpathians, modified from Matenco et al. (2013). Only the fault motions playing a role during Quaternary time are displayed. Note the potentially reactivated thick-skinned fault. The stars show the cumulative rates of vertical motion in Pleistocene to Holocene time, from Necea et al. (2013), confirmed by present-day GPS vertical motions from van der Hoeven et al. (2005). b) Apatite Helium thermochronometry ages from Necea (2010). Note that a) and b) share the same x-axis as distance along the cross-section.

4 Methods

4.1 Digital Elevation Model, preprocessing and river network

We use the publicly available ALOS World 3D 30 (AW3D30) meter resolution topographic dataset for the study (Tadono et al., 2016). It has been shown to better capture accurate channel elevations than 30m SRTM data and, in some cases, 12 m TanDEM-X topographic data (Schwanghart & Scherler, 2017; Boulton & Stokes, 2018; Mudd, 2020).

The raw DEM has some internal depressions, which spuriously stop flow routing in the DEM and therefore break the drainage area accumulation. Different solutions to filling such depressions exist, but we chose to use a carving algorithm (Lindsay, 2016). Filling algorithms tend to affect an area upstream of numerical dams or depressions, and we wish to minimize the number of pixels affected by pre-processing.

However, a preliminary step is required as AW3D30 contains a small number of pit artifacts. These can be tens of meters deep and, based on inspection of satellite imagery, appear to be correlated with reflective surfaces (the AW3D30 dataset is generated from multispectral imagery). Although their area is small enough to not significantly affect the river extraction, these artifacts affect the carving algorithm by forcing unrealistic trenches to drain them. We therefore use a localised filling algorithm on these pits prior to the carving to minimise DEM corrections while ensuring realistic flow routing. Details about the process are available in the supplementary materials.

Drainage area and flow direction is extracted using a D8 algorithm (O’Callaghan & Mark, 1984), and we extract the channel network using a drainage area threshold of 450,000

m^2 for all basins draining to the topographic mountain front in the study area (Romanian South-Eastern and Eastern Carpathians).

4.2 k_{sn} extraction

As shown in Section 2.1, k_{sn} can be represented as the gradient of χ -elevation profiles. To calculate these, we must first make some decisions about how to calculate the χ coordinate: the choice of base level (x_b), reference drainage area (A_0) and the reference concavity of the overall river network (θ_{ref}). We set $A_0 = 1$ so that the gradient in χ -elevation space is equal to k_{sn} . As demonstrated by Forte & Whipple (2018), the choice of base level affects the value of χ , but not its gradient. We therefore arbitrarily fix the base levels at the mountain front draining the eastern foreland basins.

4.2.1 k_{sn} and River concavity

We take particular care when selecting the concavity index, as only k_{sn} values extracted with a same reference concavity (θ_{ref}) can be relevantly compared. Following Niemann et al. (2001) and C. W. Wobus, Crosby, & Whipple (2006), Mudd et al. (2018), if the correct concavity index is selected, tributaries and the main stem channel should be co-linear, even in transient landscapes. We use a set of algorithms described in Mudd et al. (2018) and Hergarten et al. (2016), aiming to maximise the co-linearity of χ -elevation space for each watershed, which is then selected as the most likely value of θ_{ref} for that watershed. Uncertainty around that best fit is also calculated by calculating best fit for sub-sets of connected rivers within each watershed (Mudd et al., 2018).

4.2.2 Segmentation of χ -Elevation profiles

Once θ_{ref} has been determined, k_{sn} can be calculated using the gradient of elevation as a function of χ . Direct, pixel-by-pixel determination of k_{sn} is sensitive to inherent DEM noise and would require the use of some form of post-processing (*e.g.*, a moving average window) to exploit the results. Such a method would smooth over discontinuities such as knickpoints. Instead, we employ the algorithm described in Mudd et al. (2014), which applies a statistical method to select the most likely combination of linear segments in χ -elevation: these linear segments are predicted by the theoretical work of (L. Royden & Perron, 2013).

The Mudd et al. (2014) algorithm first selects a user-defined number of adjacent river nodes, referred to as n_{tg} . The algorithm calculates all the combinations of segments composed of a minimum amount of nodes and calculates best-fit metrics for each combination of segments. A good fit to the data is balanced against too high a number of segments (*i.e.*, over fitting) using the Akaike Information Criterion (Akaike, 1974). Each segment describes a section of river profile as:

$$z_{seg} = M_{\chi} * \chi + b_{\chi} \quad (5)$$

where $M_{\chi} = k_{sn}$ if χ has been calculated with $A_0 = 1$, and b_{χ} represents the intercept of each segment. To make sure that small-scale noise does not affect the results, the algorithm repeats this segmentation a user-defined amount of times following a Monte Carlo scheme where n_{sk} nodes are skipped in average at each iteration. The k_{sn} value for each node is the mean value of all the segment slopes involved in the calculation.

Calculating k_{sn} with the Mudd et al. (2014) algorithm relies on a certain number of subjective user-defined parameters. Some can be determined via other means, like the choice of A_0 and θ_{ref} addressed in section 4.2.1, but others need to be carefully justified as their choice will affect the segmentation process. The size of the segments is a particularly important factor to consider: it will determine the scale represented by k_{sn} variations extracted

with the algorithm. The segment size is determined by the number of nodes targeted by each algorithm iteration (n_{tg}) and the number of nodes skipped at each Monte Carlo iteration (n_{sk}). Higher values for these parameters will tend to generate larger segments, thereby averaging longer river reaches, whereas smaller values will generate smaller segments representing small-scale features. The effects of varying these parameters have been explored in detail by Gailleton et al. (2019).

4.2.3 Relative steepness index

As shown in the previous sections, calculating k_{sn} depends on a number of parameters which affect (i) the absolute value of k_{sn} and (ii) the scale it represents via the relative size of segments in the profiles. Two populations of k_{sn} , for example from different watersheds, are directly comparable only if the metric has been calculated with the same parameters (e.g. Kirby & Whipple, 2012; Hurst et al., 2019).

Different values of θ , for example, will generate different orders of magnitude of k_{sn} . Large areas, such as entire mountain ranges, will naturally have spatial variations in concavity and concavity indices (e.g. Seagren & Schoenbohm, 2019; Chen et al., 2019). In this study, we propose circumventing this limitation by (i) calculating k_{sn} for a wide range of parameters in order to represent as many processes as possible and (ii) comparing cross-parameter results with a relative steepness index.

To calculate a relative channel steepness index, we use a statistical metric called the modified z-score (T. Crosby et al., 1994), which we denote with M_i . M_i represents the statistical distribution of a population and allows us to quantify how it varies in space. The modified z-score is a nonparametric version of the z-score and suits our dataset better, as k_{sn} values are not expected to be normally distributed, particularly in a transient environment.

In this study, a population is defined by all the comparable values of k_{sn} calculated with the same parameters, namely n_{tg} , n_{sk} and θ_{ref} , and is calculated as follows:

$$M_{i,j} = \frac{0.6745 * (k_{sn,i,j} - \tilde{k}_{sn,j})}{MAD_j} \quad (6)$$

where $M_{i,j}$ is the modified z-score for pixel i and parameter value combination j . Each pixel has a channel steepness index for a given parameter combination $k_{sn,i,j}$. In addition, for each parameter combination we calculate the median channel steepness index, $\tilde{k}_{sn,j}$ and the median absolute deviation (MAD) for that parameter combination MAD_j :

$$MAD_j = median(|k_{sn,i,j} - \tilde{k}_{sn,j}|) \quad (7)$$

$M_{i,j}$ quantifies the absolute values of each population in regards to its median. $M_{ik_{sn}} = 0$ equals to the median and higher and lower values denote respectively higher and lower samples compare to the overall population. This method is traditionally widely used to detect outliers in large datasets (e.g. Giustacchini et al., 2017). Because all values of $M_{i,j}$ are normalized to the median values and median absolute deviations of each parameter value combination, we can use these to compare relative channel steepness amongst k_{sn} data with different parameter values. We therefore refer to the $M_{i,j}$ data as the “relative channel steepness” in all our figures, with values greater than zero representing parts of the channel network that have steepness greater than the median, and values less than zero representing parts of the channel network that are gentler than the median k_{sn} values.

4.3 Rock strength

We apply a semi-qualitative approach to estimate rock strength. First, the extent of the tecto-lithologic units is estimated using the compilation of 1:50,000, 1:200,000 and 1:500,000 geological maps (published by the Geological Institute of Romania), Maţenco et al. (2010) and Maţenco (2017). The Ukrainian section of the map has been completed and extrapolated using the extent of tectonic units in Andreucci et al. (2015), with some spatial approximations and unit grouping match nomenclature in the different datasets. We also acknowledge that lithostratigraphic variation can occur within each tectonic unit, and we take account of potential internal major changes using (e.g. Maţenco & Bertotti, 2000), which compiles local stratigraphic information (e.g. Joja et al., 1968; Săndulescu, 1984). The chosen grouping allows us to (i) follow the continuous northward evolution of channel steepness along similar units, and (ii) encompass large-scale signals.

We then measure the uniaxial compressive strength of the rock through the study area. Schmidt hammer measurements were carried out in the field on rock outcrops, where we focused on fresh rock surfaces. The Schmidt hammer, type N in this study, records a “rebound value” between 10 and 100 where higher values denote high elastic strength of the rock. We also record the outcrops where the rock was too soft to be tested, *i.e.* where the Schmidt hammer did not encounter enough resistance from the rock to return a measurement. The rebound value can be converted to compressive strength using a chart provided and calibrated with the equipment used in the field.

Each measurement point represents the median value of 30 to 50 Schmidt hammer impacts on the same spot. Several points are tested per outcrop in order to (i) ensure the consistency of the method and (ii) check local variability and potential heterogeneity in the fracture network or weathering intensity.

5 Results

5.1 Rock strength

We collected a total of 347 rock strength measurements across the tectonic units in the Southeastern Carpathians (SEC). The results are quantified using two different metrics: (i) the rebound values (medians and quartiles for each tectonic unit excluding the non-responsive data points) and (ii) the proportion of non-responsive measurements for each tectonic unit (Figure 3).

Rock strength measurements show a wide range of rock strength values. The range in values reflects the stratified nature of the lithologic units where softer rocks are interbedded with harder rocks. However, the data does suggest a trend: we can isolate two different groups of lithologic units that behave differently. The first group includes the Ceahlău-Serevin, Audia, Macla, Tarcau and Marginal Folds units which show higher rebound values and fewer measurements resulting in a non-response from the Schmidt hammer as a proportion of the total measurements. The second group includes the two frontal units, the Subcarpathians and the Focşani Basin, with lower rebound values and higher proportions of non-responsive measurements.

These results are consistent with qualitative field observations. The first group shows more resistant lithofacies and crops out more frequently in the landscape than the second, which shows fewer, thinner and sparser resistant layers.

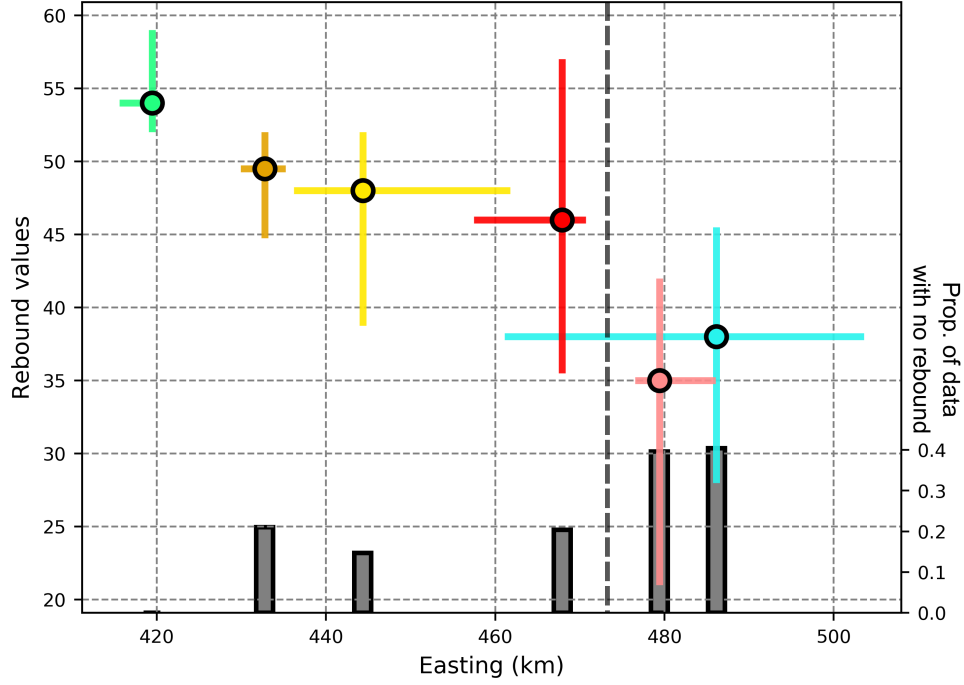


Figure 3. Schmidt hammer rebound values summarising the measurements across the Romanian Carpathians. The color of data points corresponds to the tectonic units on the location map (Fig.1). The data points represent the median rebounds values, and the error bars the first and third quartiles, respectively. The proportion of non-responsive points is also displayed, as an indirect proxy for the proportion of weak rocks within each unit.

5.2 Concavity index

Ranges of most likely θ_{ref} values for all the basins outlined in Figure 1 are shown in Figure 4 by (i) northing position in the horizontal axis, as a rough proxy for tectonic activity in the Eastern and Southeastern Carpathians (see section 3) and (ii) the median and quartiles of the most likely values on the vertical axis.

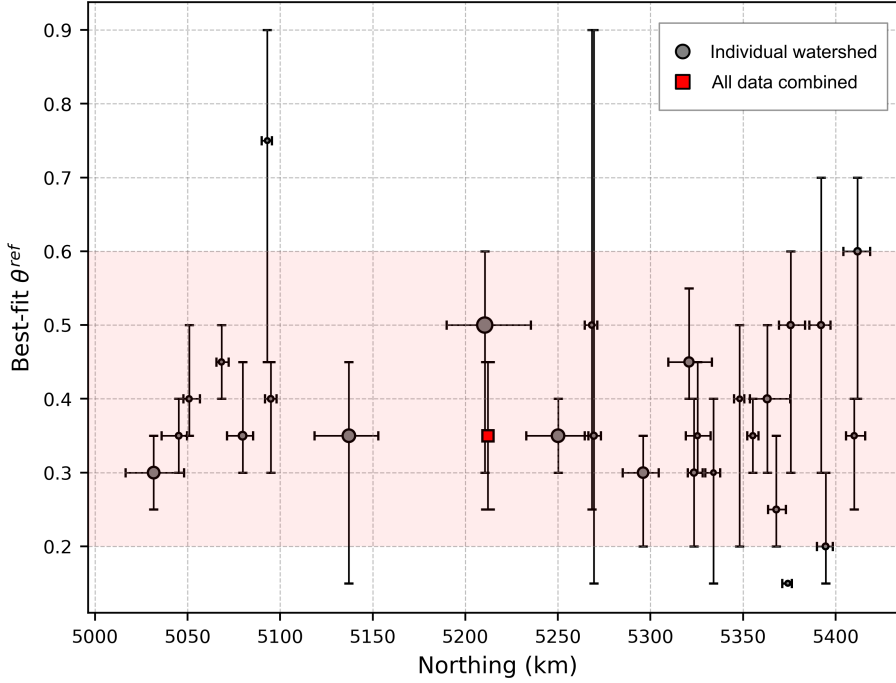


Figure 4. Concavity ranges calculated in the study area. Each point represents a single basin, where the x axis shows the median and quartiles of the northing (in km UTM zone 35), and the y axis shows the median and quartiles of all the best-fits for all the different combination of river tested for each basins. The red square represents a compilation of all the data within the study area, the red shading encompasses the selected range of θ_{ref} for this study.

The results show several trends: Across all studied basins, we find that the concavity indices have a median of 0.35 ± 0.10 (red square in Figure 4) for our study area. In the South-eastern Carpathians (basins with northing values ranging from 5000 to 5100 km, see Fig. 1), the range of values is narrower than in the Eastern Carpathians (basins with northing values greater than 5100 km). The smaller basins within the South-Eastern Carpathians, mainly draining the frontal units (Focşani Basin), tend to show higher concavity indices than larger basins. Concavity indices in the Eastern Carpathians (EC) are more heterogeneous than in other parts of the study area. On the basis of these data, we chose the range 0.2 - 0.6 for investigating the relative distribution of k_{sn} through our landscape, as it includes all the most likely values in individual basins (excluding two outliers) and most of the interquartile values (fig.4).

5.3 Relative channel steepness

We calculated k_{sn} for 486 different sets of parameters (θ^{ref} from 0.2 to 0.6 with a spacing of 0.05, n_{tg} from 20 to 100 with a spacing of 10 and n_{sk} from 0 to 4 with a spacing of 1 and for $n_{sk} = 10$). For each individual set, we calculated the relative steepness index from our combined dataset, resulting in 490,636,671 data points.

5.3.1 Regional distribution of channel steepness

Figure 5 shows the relative steepness index as a function of the northing coordinate. This provides an overview of channel steepness in regards to the different areas of differential tectonics suggested in section 3. The data is noisy, however, and does not show an obvious N-S trend. There is a sharp increase in the relative steepness index between northing values of 5000 km and 5030 km, which may be linked to the bending of the mountain range and incorporating a few and unrepresentative data points in the extreme South of Buzau watershed (Fig.1). Three regions host steep channels compared to the rest of the landscape: (i) The Focșani Basin area (northing 5000 to 5080 kilometers, HS1 on Fig.6 and Fig. 5), (ii) in the heart of the EC (northing 5125 to 5240 kilometers, HS2 on Fig.6 and Fig. 5), and (iii) a less prominent steep area in the Northeastern Carpathians from 5340 kilometers. These three areas are connected by two regions of lower relative steepness.

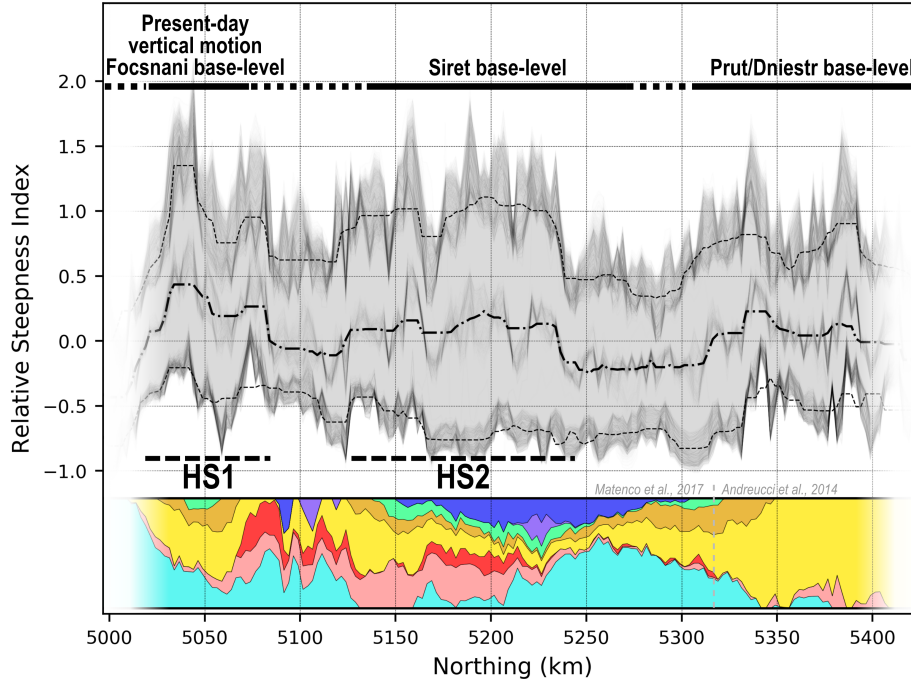


Figure 5. Relative steepness index binned by northing coordinates. The binning size is 2500m in UTM zone 35 and is used as a rough proxy for tectonic activity to differentiate the Southeastern Carpathians from the rest of the Eastern Carpathians (see section 3). Transparent thin grey lines represent each different population of relative channel steepness calculated for different combinations of parameters (see section 4.2.3), and the thicker black lines are a running median window across 9 points. Bottom lines, middle and top dashed lines are respectively the third quartiles, medians and first quartiles of all values within each bin. The bottom figure represents the proportion of lithology across the landscape for each northing point, using the same colors as figure 1 to identify the different tectonic units.

The absence of a monotonic N-S trend is also expressed in a map view (Fig.6) where the median of all the relative steepness indices suggest a compartmentalised dataset. A clear

N-S mid-range linear feature sharply separates an eastern region of lower steepness and a western region of higher steepness. This main break in steepness is labelled MBiS (Main Break in Slope) on Fig.6. The sharpness of the contact is less clear south of 5160 km. Other less clearly expressed trends can be observed with this map view. (i) Within the Western region of high steepness, high patches stand out, particularly at kilometers 5030 (HS1), 5130. (ii) Within that same region, localised patches of low values express the presence of high-elevation low-gradient (HELG) valleys in the Buzau, Trotus, Bistrita and Prut watersheds (labelled HELG on Fig.6). (iii) A region of lower steepness occurs within the Moldova watershed, with a sharp decrease of the values occurring at the drainage boundary between the Bistrita and Moldova watersheds.

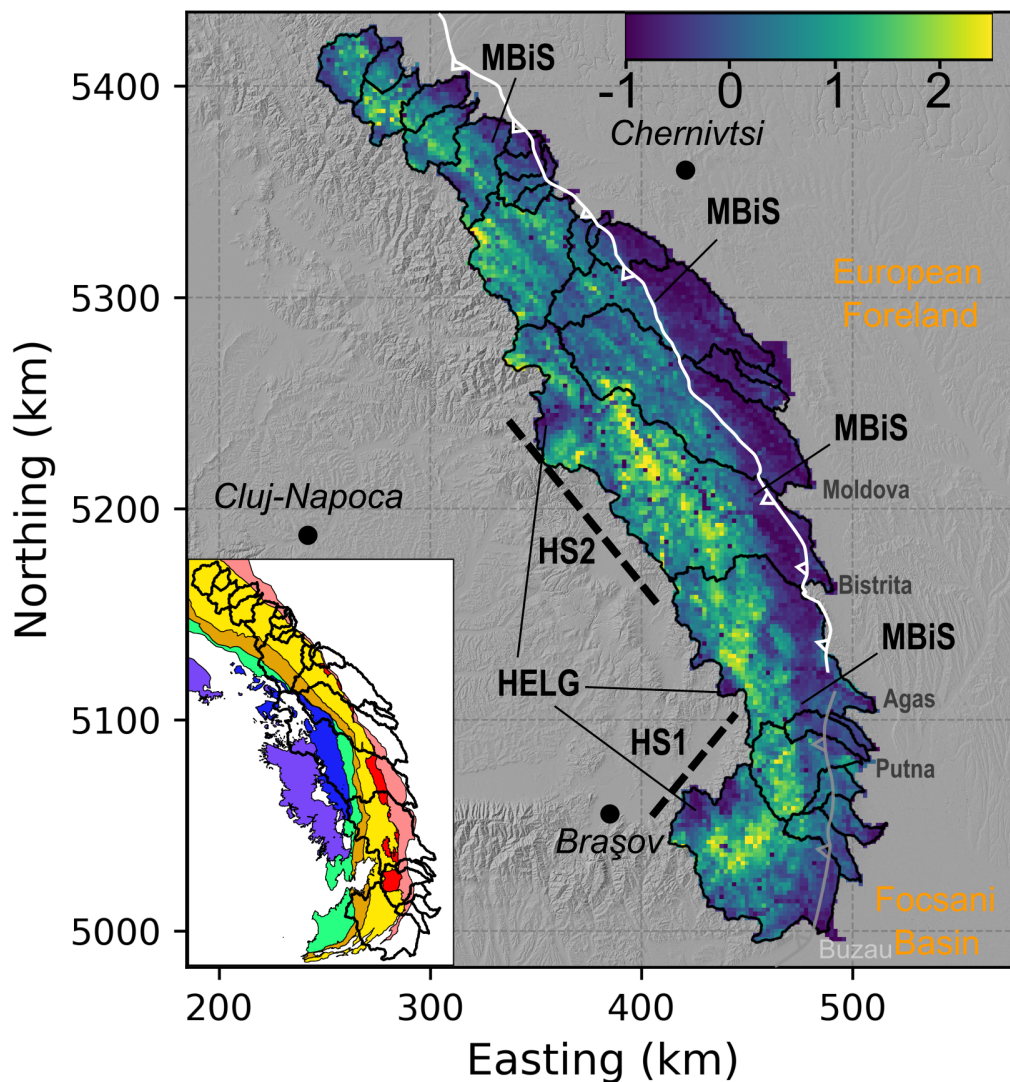


Figure 6. Relative steepness index binned in 2D using median binning of the median of relative steepness indices calculated for every set of parameters. The first and third quartile maps are available in the Supplemental Materials.

5.3.2 Channel steepness as a function of lithology and tectonic units

Figure 7 shows relative channel steepness plotted as a function of the northing coordinate for each litho-tectonic unit. Large-scale trends stand out: the Western Focșani Basin and its northern foredeep continuation, as well as the Subcarpathians and Marginal folds nappes show a gradual northward decay of their values, with a flattening or insignificant increase North to km 5200 (*i.e.* North of the Bistrita watershed). The Tarcau nappe shows high values until the same km 5200 while sharply decreasing northwards. The Audia/Macla/Convolute Flysh and Ceahlău-Severin nappes behave differently with (i) low, heterogeneous values in the Southeastern Carpathians, (ii) a peak around the same kilometer 5200 in the Bistrita watershed (Fig.1) (iii) followed by a sharp decrease until kilometer 5300 (*i.e.* the Northern part of the Siret baselevel) and (iv) high values in the northernmost area, linked to Prut and Dniestr base level, North to kilometre 5300. Finally, the basement rocks of the Dacia units locally impose patches of high relative steepness in the Eastern Carpathians where these rocks are largely exposed.

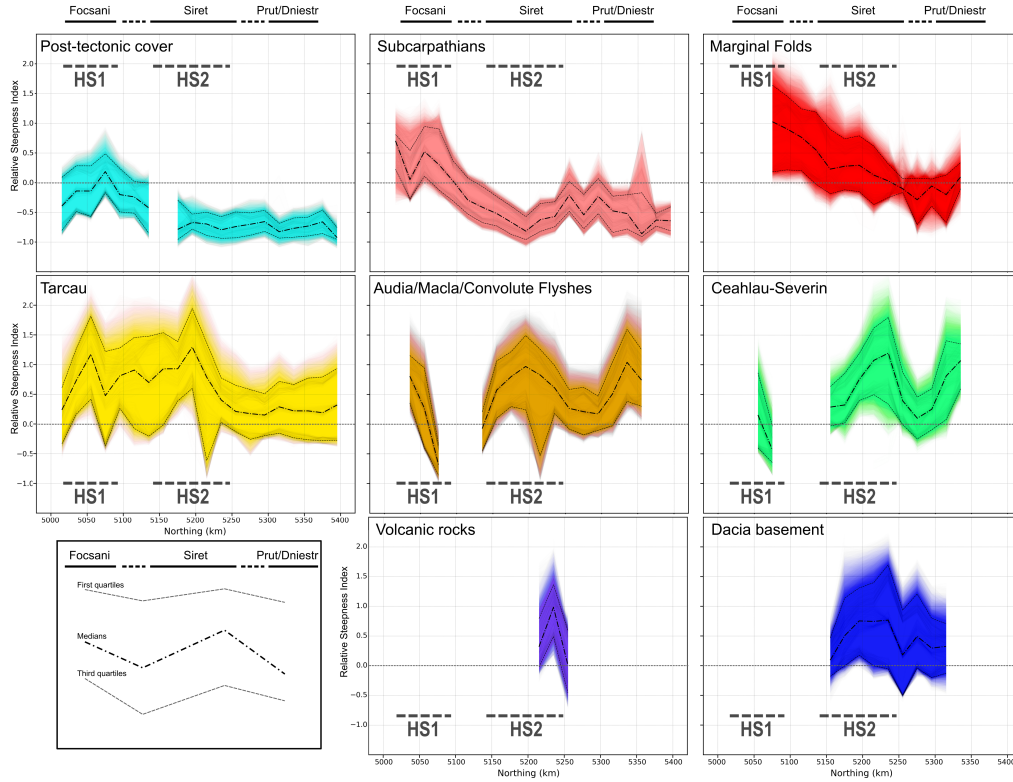


Figure 7. Relative steepness index binned by litho-tectonic units and by northing, using the same approach as fig.5. For each litho-tectonic unit, relative channel steepness indices calculated for all the different sets of parameters are displayed in fine shaded lines binned by northing (25000 m in UTM zone 35). The thicker lines are moving median windows over the first quartiles, medians and third quartiles (3 points). The colors correspond to the tectonic units in Fig.1.

Figure 7 also highlights multiple notable behaviors differing from a northward monotonic decay as one moves away from the active vertical motions of the Southeastern Carpathians. (i) Although the Subcarpathian nappe has its highest values in the Focșani area, it also displays a local peak north of kilometer 5200, denoting a greater proportion of steeper

channels within the Subcarpathian nappe in the area. Note that the exposed surface of this unit decreases northward (Fig.5), increasing the potential effect of noise on the data. (ii) The Tarcau nappe shows a sharp rather than gradual northward decay, as well as high variability. (iii) The Audia/Macla and Ceahlău-Severin units do not show northward decay in channel steepness but variable local trends. They also outcrop less within the river network (Fig.5).

6 Discussion

6.1 Spurious tectonic signals

A prominent break in channel steepness can be seen in Figure 6 to the east of the main drainage divide that extends along the entire N-S axis of the study area. Section 2.2 highlighted tectonics as a common forcing generating similar features. In the Carpathians, recent tectonic activity is concentrated in the southeastern bend of the mountain range (see 3). The break in channel steepness observed in Figure 6 extends far beyond the region where deformation is inferred from other independent proxies, and could be used as an argument for extrapolating recent tectonic activity to the North. However, our rock strength data (Figure 3), combined with apparent tectonic inactivity north of the South-Eastern Carpathians, point to lithology as the main driver of the break in channel steepness. This is concentrated where the evaporite-rich and highly fractured rocks of the Subcarpathians and sandstone-rich Tarcau and Marginal fold units lie in contact (e.g. Yanites et al., 2017; Bernard et al., 2019). This highlights the danger of extracting channel metrics at large scale without taking local lithological context into account.

This line of reasoning also suggests lithology as a control on more local channel steepness contrasts, for example: (i) The patch of high relative channel steepness at the top of the Bistrita watershed, described in Section 5.3. Its boundaries correspond to the mostly magmatic rocks of the Dacia basement units and the volcanic rocks linked to Neogene volcanism. (ii) Very sharp and significant drop of relative steepness index (Fig.6 and 7) occurs within the Tarcau nappe around Northing kilometres 5200 to 5250 (see Fig.7). Local litho-stratigraphic data (Maţenco & Bertotti, 2000) highlights that this also corresponds to a lithological change from coarse-grained resistant sandstones in the Bistrita valley to finer-grained, often shaly turbidites in the Moldova valley (see Fig.6). It additionally collapses nearly perfectly with the drainage divide between the Bistrita and Moldova watersheds (Fig.6); this represents another possible expression of lithologic forcing by “pinning” drainage divides on resistant rocks (e.g. Seagren & Schoenbohm, 2019; Bernard et al., 2019). (iii) Low steepness values are observed at the highest, westernmost part of the Bistrita watershed, corresponding to a switch from the resistant metamorphic rocks of the Dacia basement to softer sedimentary rocks belonging to the Transylvanian Basin (Maţenco, 2017).

Figure 8 and 9 illustrates how global and local lithologic forcings can generate relative steepness contrasts which can potentially lead to spurious tectonic interpretations.

6.2 Integration of relative channel steepness index in the tectonic model

Knowing that lithology can influence the patterns of relative channel steepness, we must then consider strategies for extracting tectonic signals from lithologically complex terrain (see Section 5.3.2 and 6.3).

Within litho-tectonic units at the eastern edge of the range, *i.e.* the whole area eastern to the main break of steepness (MBIS on Fig.6), we find higher values of relative channel steepness index in the South Eastern Carpathians (HS1 area of units Subcarpathians and Post-Tectonic on Figure 7). This suggests that there is a tectonic signal of increasing rock uplift rates from north to south in the frontal units, consistent with what was suggested by structural and exhumation studies. This pattern is particularly clear for the Marginal

Folds, the Subcarpathians and the Focșani basin/Post-Tectonics units, with all showing a monotonic northward decrease in channel steepness. When looking at channel steepness patterns over the entire mountain range, the changes in steepness from different lithologies are greater than the N–S trends within the frontal litho-tectonic units, highlighting how tectonic patterns may be masked by lithologic contrasts in rock erodibility.

Previous studies (see Section 3) also suggested an eastward gradient in vertical motions within the Southeastern Carpathians by reactivating deep faults that do not reach the surface. As we suggest that the sharpness of the channel steepness contrast is due to lithology, our data is compatible with this previous tectonic interpretation. It demonstrates that the tectonic signal is hidden behind the lithologic one but is still expressed in the topography. The most prominent expression of this mixed signal is the 1000m high mountain at the front of the Putna valley made of very soft sedimentary rocks.

Patterns of relative steepness index within the Tarcau unit are more ambiguous than the others. Here, the relative steepness index does not show a gradual decrease northward like other units. It sustains higher values northern than other units before a sharp drop. Given the fact that the Tarcau units show the hardest rocks in the Southeastern Carpathians thin-skinned sediments and contain a significant change of lithology northward, we suggest that the lithologic forcings overprint the tectonic one in this unit.

6.3 Non lithologic low-gradient area within the South-Eastern Carpathians

Although rock hardness measurements in the South-Eastern Carpathians do not suggest significant lithologic contrasts between the Ceahlău-Severin, Audia/Macla and Tarcau units (Fig.3), the upper parts of the Buzau basin show low values of channel steepness. We explain this different behavior using local data from these units. (i) Thermochronometers from Merten et al. (2010) have suggested an older and lower magnitude exhumation of these units through time in the South-East Carpathians (in the Buzau watershed), which can be related to long-wavelength of exhumation related to slab-retreat type of processes (e.g. Picotti & Pazzaglia, 2008; Mațenco, 2017). (ii) Several authors (Fielitz & Seghedi, 2005; Necea, 2010; ter Borgh, 2013) suggested a drainage reorganisation explaining these high elevation low-gradient valleys. Our dataset is consistent with these previous observations, showing steep “aggressive” (*sensu* Willett et al. (2014)) rivers in the Buzau watershed juxtaposed with an upstream low gradient, diffusive landscape. These values are at odds with the regional pattern of tectonic activity, *i.e.* high tectonic activity in the South-Eastern Carpathians and post-collisional decay in the Eastern Carpathians, and bias the global distribution of relative channel steepness (Fig.5 and 6) by reducing the regional values.

These two factors can be linked, as tectonics is a common driver for drainage divide reorganisation (e.g. Willett et al., 2014; Giachetta & Willett, 2018; Seagren & Schoenbohm, 2019). Fig.9 summarises the local signals observed within the Buzau watershed, illustrating the diversity of local expression of channel steepness.

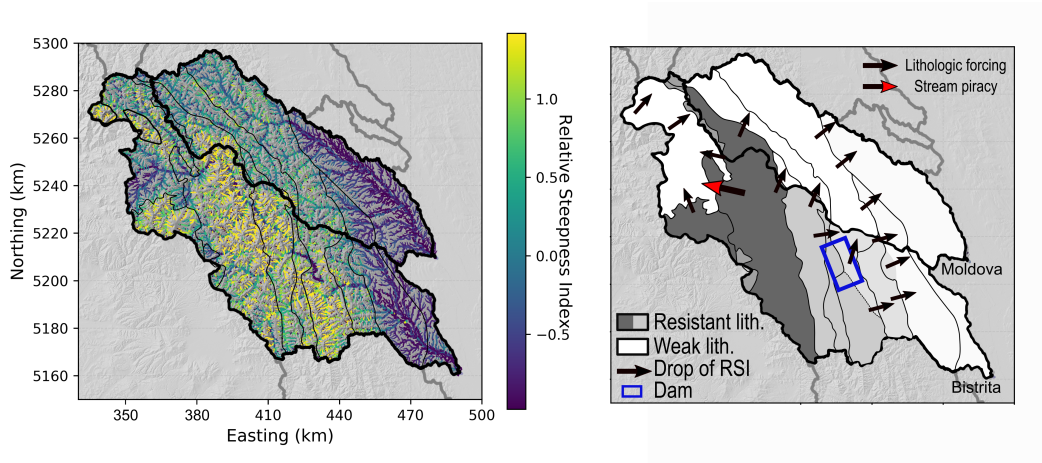


Figure 8. Illustration of the diversity of forcings generating potentially spurious tectonic signals by inducing steepness contrasts within the Eastern Carpathians, in the watersheds Bistrita and Moldova.

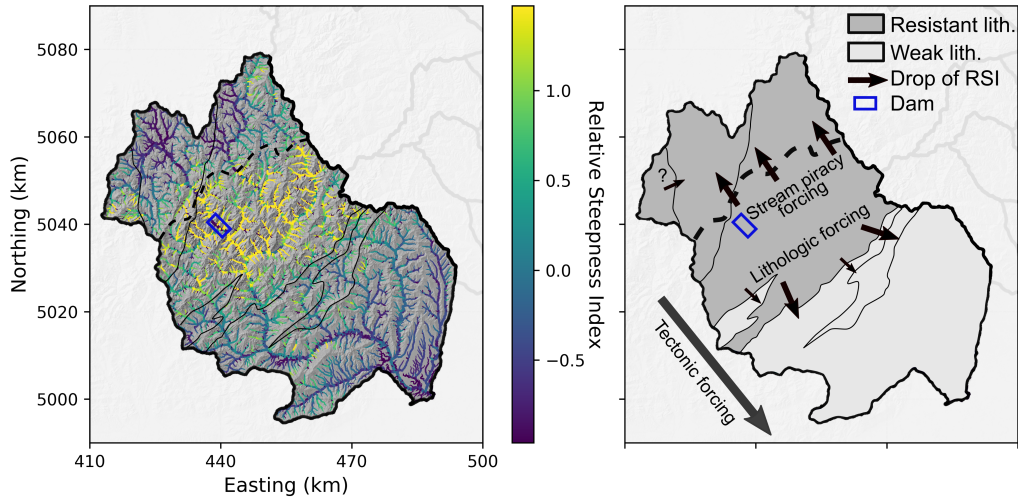


Figure 9. Illustration of the diversity of local expression of tectonics, lithologic and stream piracy forcings in the South-Eastern Carpathians within the Buzau watershed.

7 Conclusions

Detecting tectonic signals from channel steepness can be challenging challenged lithologic heterogeneity, a common feature of mountain ranges. This overprints on the tectonic signals and potentially hides or falsifies it. Additionally to this, exploring channel steepness across a wide geographical range will almost inevitably encompass basins with differing concavities, which can cloud interpretation of channel steepness. In this study, we successfully unravel tectonics and lithologic signals from channel steepness in the Eastern and Southeastern Carpathians, a range showing different lithologic and tectonic gradients across multiple scales.

We find that the concavity index, which affects normalized steepness values (k_{sn}) varies between approximately 0.2 and 0.6 in the Eastern and Southeastern Carpathians. Choosing a single reference concavity might result in misleading k_{sn} values. We therefore developed a method for calculating relative steepness that can be applied across basins with different concavities using a modified $z - score$ method that takes into account the non-normal distribution of channel steepness values across all catchments.

The first order values of relative steepness across the range show a large contrast between the gentle eastern front of the range and steep areas near the drainage divide. The presumed N–S trends in uplift rates are not obviously reflected in the relative steepness data at this scale. However, when we group steepness by litho-tectonic units, we find that different units have different relative steepness.

We collected rock hardness data across the litho-tectonic units and find that the hardness can be broadly grouped into hard and soft units. This grouping is reflected in the relative channel steepness data.

Separating the relative steepness by litho-tectonic units, a N–S spatial pattern appears. In the units at the mountain front, this pattern is most clear: relative steepness is highest in the part of the mountain range where thermochronometers have recorded the highest long-term exhumation rates. In addition, steepness data confirms the migration of the surface uplift pattern towards the East, where thermochronometers show unreset ages and cannot be used to estimate exhumation. Without accounting for lithology, this tectonic signal would have been entirely masked by differences in rock hardness. Spatial trends in the harder rocks toward the peaks of the range show more localised patterns: for example, high-elevation low-gradient valleys expressing localised stream piracy and lithologic variations within hard units explaining other less prominent contrasts in relative steepness.

Evaluation of variable rock uplift from channel steepness measurements on the scale of an entire mountain range is challenged by the variability in rock strength and the concavity of the channel profile. Through characterisation of channel concavities and independent measures of rock strength, it is possible to isolate for the role of tectonics versus lithology.

Acknowledgments

Schmidt-hammer data table can be found at <https://doi.org/10.7488/ds/2950>. The softwares used for topographic analysis are available at <https://github.com/LSDtopotools>. Boris Gailleton was funded by European Union initial training grant 674899 SUBITOP. and Emma L.S. Graf was supported by NERC grant NE/L002558/1. We thank Laura Quick, Antoine Auzemery and Guillaume Goodwin for help with field data collection.

References

- Ahnert, F. (1970). Functional relationships between denudation, relief, and uplift in large, mid-latitude drainage basins. *American Journal of Science*, 268(3), 243–263. doi: 10.2475/ajs.268.3.243
- Akaike, H. (1974). A New Look at the Statistical Model Identification. *IEEE Transactions on Automatic Control*, 19(6), 716–723. doi: 10.1109/TAC.1974.1100705
- Allen, P. A. (2017). *Sediment routing systems : the fate of sediment from source to sink*. Cambridge University Press.
- Andreucci, B., Castelluccio, A., Corrado, S., Jankowski, L., Mazzoli, S., Szaniawski, R., & Zattin, M. (2015). Interplay between the thermal evolution of an orogenic wedge and its retro-wedge basin: An example from the Ukrainian Carpathians. *Bulletin of the Geological Society of America*, 127(3-4), 410–427. doi: 10.1130/B31067.1
- Arrowsmith, J. R., Rhodes, D. D., & Pollard, D. D. (1998). Morphologic dating of scarps formed by repeated slip events along the San Andreas Fault, Carrizo Plain, California.

- Journal of Geophysical Research: Solid Earth*, 103(B5), 10141–10160. doi: 10.1029/98jb00505
- Avouac, J. P., & Burov, E. B. (1996). Erosion as a driving mechanism of intracontinental mountain growth. *Journal of Geophysical Research: Solid Earth*, 101(B8), 17747–17769. doi: 10.1029/96jb01344
- Beaumont, C., Fullsack, P., & Hamilton, J. (1992). Erosional control of active compressional orogens. In *Thrust tectonics* (pp. 1–18). Dordrecht: Springer Netherlands. doi: 10.1007/978-94-011-3066-0_1
- Belayouni, H., Di Staso, A., Guerrera, F., Martín Martín, M., Miclu, C., Serrano, F., & Tramontana, M. (2009). Stratigraphic and geochemical study of the organic-rich black shales in the Tarcu Nappe of the Moldavidian Domain (Carpathian Chain, Romania). *International Journal of Earth Sciences*, 98(1), 157–176. doi: 10.1007/s00531-007-0226-7
- Bernard, T., Sinclair, H. D., Gailleton, B., Mudd, S. M., & Ford, M. (2019). Lithological control on the post-orogenic topography and erosion history of the Pyrenees. *Earth and Planetary Science Letters*, 518, 53–66. doi: 10.1016/j.epsl.2019.04.034
- Bezerra, D. P. (2018). The pattern and style of landscape evolution in post-orogenic settings. (*Doctoral thesis, School of Geographical and Earth Sciences, College of Science and Engineering, University of Glasgow, Glasgow, UK*), 271.
- Bierman, P., & Steig, E. J. (1996). Estimating Rates of Denudation Using Cosmogenic Isotope Abundances in Sediment. *Earth Surface Processes and Landforms*, 21(2), 125–139. doi: 10.1002/(sici)1096-9837(199602)21:2<125::aid-esp511>3.0.co;2-8
- Bocin, A., Stephenson, R., Mocanu, V., & Mațenco, L. (2009). Architecture of the south-eastern Carpathians nappes and Focsani Basin (Romania) from 2D ray tracing of densely-spaced refraction data. *Tectonophysics*, 476(3-4), 512–527. doi: 10.1016/j.tecto.2009.07.027
- Bocin, A., Stephenson, R., Tryggvason, A., Panea, I., Mocanu, V., Hauser, F., & Mațenco, L. (2005). 2.5D seismic velocity modelling in the south-eastern Romanian Carpathians Orogen and its foreland. *Tectonophysics*, 410(1-4), 273–291. doi: 10.1016/j.tecto.2005.05.045
- Bokelmann, G., & Rodler, A. (2014). Nature of the Vrancea seismic zone (Eastern Carpathians) New constraints from dispersion of first-arriving P-waves. *Earth and Planetary Science Letters*, 390, 59–68. doi: 10.1016/j.epsl.2013.12.034
- Boulton, S. J., & Stokes, M. (2018). Which DEM is best for analyzing fluvial landscape development in mountainous terrains? *Geomorphology*, 310, 168–187. doi: 10.1016/j.geomorph.2018.03.002
- Bălțeanu, D., Chendeș, V., Sima, M., & Enciu, P. (2010). A country-wide spatial assessment of landslide susceptibility in Romania. *Geomorphology*, 124(3-4), 102–112. doi: 10.1016/j.geomorph.2010.03.005
- Campforts, B., Vanacker, V., Herman, F., Vanmaercke, M., Schwanghart, W., Tenorio, G. E., ... Govers, G. (2019). Lithology and orographic precipitation control river incision in the tropical Andes. *Earth Surface Dynamics Discussions*, 2019, 1–43. doi: 10.5194/esurf-2019-48
- Chen, S.-A., Michaelides, K., Grieve, S. W. D., & Singer, M. B. (2019). Aridity is expressed in river topography globally. *Nature*, 573(7775), 573–577. doi: 10.1038/s41586-019-1558-8
- Codilean, A. T., Munack, H., Cohen, T. J., Saktura, W. M., Gray, A., & Mudd, S. M. (2018). OCTOPUS: An open cosmogenic isotope and luminescence database. *Earth System Science Data*, 10(4), 2123–2139. doi: 10.5194/essd-10-2123-2018
- Cristea, A.-I. (2014). Assessment of recent tectonic evolution and geomorphic response in SE Carpathians (Romania) using hypsometric analysis. *GEOREVIEW: Scientific Annals of Stefan cel Mare University of Suceava. Geography Series*, 24(1), 76–88. doi: 10.4316/GEOREVIEW.2014.24.1.265
- Cristea, A. I. (2015). Spatial analysis of channel steepness in a tectonically active region: Putna river catchment (South-Eastern Carpathians). *Geographia Technica*, 10(1), 19–27.

- Crosby, B. T., & Whipple, K. X. (2006). Knickpoint initiation and distribution within fluvial networks: 236 waterfalls in the Waipaoa River, North Island, New Zealand. *Geomorphology*, 82(1-2), 16–38. doi: 10.1016/j.geomorph.2005.08.023
- Crosby, T., Iglewicz, B., & Hoaglin, D. C. (1994). How to Detect and Handle Outliers. *Technometrics*, 36(3), 315. doi: 10.2307/1269377
- Csontos, L., & Vörös, A. (2004). *Mesozoic plate tectonic reconstruction of the Carpathian region* (Vol. 210) (No. 1). doi: 10.1016/j.palaeo.2004.02.033
- D., S. H., J., C. B., A., A. P., & B., W. A. (1991). Simulation of Foreland Basin Stratigraphy using a diffusion model of mountain belt uplift and erosion: An example from the central Alps, Switzerland. *Tectonics*, 10(3), 599–620. doi: 10.1029/90TC02507
- de Lapparent, A. (1896). *Leçons de géographie physique*. Paris: Masson et c', éditeurs.
- de Lapparent, A. A. C. (1907). *Leçons de géographie physique*. Masson.
- DiBiase, R. A., Whipple, K. X., Heimsath, A. M., & Ouimet, W. B. (2010). Landscape form and millennial erosion rates in the San Gabriel Mountains, CA. *Earth and Planetary Science Letters*, 289(1-2), 134–144. doi: 10.1016/j.epsl.2009.10.036
- Duvall, A. (2004). Tectonic and lithologic controls on bedrock channel profiles and processes in coastal California. *Journal of Geophysical Research*, 109(F3), 1–18. doi: 10.1029/2003jf000086
- Eizenhöfer, P. R., McQuarrie, N., Shelef, E., & Ehlers, T. A. (2019). Landscape Response to Lateral Advection in Convergent Orogens Over Geologic Time Scales. *Journal of Geophysical Research: Earth Surface*, 124(8), 2056–2078. doi: 10.1029/2019jf005100
- Fielitz, W., & Seghedi, I. (2005). Late Miocene-Quaternary volcanism, tectonics and drainage system evolution in the East Carpathians, Romania. *Tectonophysics*, 410(1-4), 111–136. doi: 10.1016/j.tecto.2004.10.018
- Flint, J. J. (1974). Stream gradient as a function of order, magnitude, and discharge. *Water Resources Research*, 10(5), 969–973. doi: 10.1029/WR010i005p00969
- Forte, A. M., & Whipple, K. X. (2018). Criteria and tools for determining drainage divide stability. *Earth and Planetary Science Letters*, 493, 102–117. doi: 10.1016/j.epsl.2018.04.026
- Forte, A. M., Yanites, B. J., & Whipple, K. X. (2016). Complexities of landscape evolution during incision through layered stratigraphy with contrasts in rock strength. *Earth Surface Processes and Landforms*, 41(12), 1736–1757. doi: 10.1002/esp.3947
- Gabet, E. J. (2019). Lithological and structural controls on river profiles and networks in the northern Sierra Nevada (California, USA). *GSA Bulletin*. doi: 10.1130/b35128.1
- Gaillardet, B., Mudd, S. M., Clubb, F. J., Peifer, D., & Hurst, M. D. (2019). A segmentation approach for the reproducible extraction and quantification of knickpoints from river long profiles. *Earth Surface Dynamics*, 7(1), 211–230. doi: 10.5194/esurf-7-211-2019
- Giachetta, E., & Willett, S. D. (2018). Effects of river capture and sediment flux on the evolution of plateaus: Insights from numerical modeling and river profile analysis in the upper blue Nile catchment. *Journal of Geophysical Research: Earth Surface*, 123(6), 1187–1217. doi: 10.1029/2017JF004252
- Gilbert, G. K. (1877). *Geology of the Henry Mountains* (USGS Unnumbered Series). Washington, D.C.: Government Printing Office.
- Giustacchini, A., Thongjuea, S., Barkas, N., Woll, P. S., Povinelli, B. J., Booth, C. A., ... Mead, A. J. (2017). Single-cell transcriptomics uncovers distinct molecular signatures of stem cells in chronic myeloid leukemia. *Nature Medicine*, 23(6), 692–702. doi: 10.1038/nm.4336
- Goren, L. (2016). A theoretical model for fluvial channel response time during time-dependent climatic and tectonic forcing and its inverse applications. *Geophysical Research Letters*, 43(20), 10,753–10,763. doi: 10.1002/2016GL070451
- Gröger, H. R., Fügenschuh, B., Tischler, M., Schmid, S. M., & Foeken, J. P. (2008). Tertiary cooling and exhumation history in the Maramures area (internal eastern Carpathians, northern Romania): Thermochronology and structural data. *Geological Society Special Publication*, 298(1), 169–195. doi: 10.1144/SP298.9

- Hack, J. (1957). *Studies of longitudinal stream profiles in Virginia and Maryland*. USGS Professional Paper 249.
- Hack, J. T. (1960). Interpretation of erosional topography in humid temperate regions. *American Journal of Science*, 258-A(A), 80–97.
- Harel, M. A., Mudd, S. M., & Attal, M. (2016). Global analysis of the stream power law parameters based on worldwide 10 Be denudation rates. *Geomorphology*, 268, 184–196. doi: 10.1016/j.geomorph.2016.05.035
- Hauser, F., Raileanu, V., Fielitz, W., Dinu, C., Landes, M., Bala, A., & Prodehl, C. (2007). Seismic crustal structure between the Transylvanian Basin and the Black Sea, Romania. *Tectonophysics*, 430(1-4), 1–25. doi: 10.1016/j.tecto.2006.10.005
- Hergarten, S., Robl, J., & Stuwe, K. (2016). Tectonic geomorphology at small catchment sizes—extensions of the stream-power approach and the x method. *Earth Surface Dynamics*, 4(1), 1–9. doi: 10.5194/esurf-4-1-2016
- Hurst, M. D., Grieve, S. W., Clubb, F. J., & Mudd, S. M. (2019). Detection of channel-hillslope coupling along a tectonic gradient. *Earth and Planetary Science Letters*, 522, 30–39. doi: 10.1016/j.epsl.2019.06.018
- Hurst, M. D., Mudd, S. M., Attal, M., & Hilley, G. (2013). Hillslopes record the growth and decay of landscapes. *Science*, 341(6148), 868–871. doi: 10.1126/science.1241791
- Ismail-Zadeh, A., Mațenco, L., Radulian, M., Cloetingh, S., & Panza, G. (2012). Geodynamics and intermediate-depth seismicity in Vrancea (the south-eastern Carpathians): Current state-of-the art. *Tectonophysics*, 530-531, 50–79. doi: 10.1016/j.tecto.2012.01.016
- Ivan, M. (2007). Attenuation of P and pP waves in Vrancea area - Romania. *Journal of Seismology*, 11(1), 73–85. doi: 10.1007/s10950-006-9038-7
- Jipa, D. C., & Olariu, C. (2013). Sediment routing in a semi-enclosed epicontinental sea: Dacian Basin, Paratethys domain, Late Neogene, Romania. *Global and Planetary Change*, 103(1), 193–206. doi: 10.1016/j.gloplacha.2012.06.009
- Joja, T., Mutihac, V., & Muresan, M. (1968). *Crystalline-Mesozoic and Flysch Complexes of the East Carpathians (Northern Sector)*. Geological Institute.
- Kirby, E., & Whipple, K. X. (2012). *Expression of active tectonics in erosional landscapes* (Vol. 44). doi: 10.1016/j.jsg.2012.07.009
- Kirby, E., Whipple, K. X., Tang, W., & Chen, Z. (2003). Distribution of active rock uplift along the eastern margin of the Tibetan Plateau: Inferences from bedrock channel longitudinal profiles. *Journal of Geophysical Research: Solid Earth*, 108(B4), 2217. doi: 10.1029/2001jb000861
- Lal, D. (1991). Cosmic ray labeling of erosion surfaces: in situ nuclide production rates and erosion models. *Earth and Planetary Science Letters*, 104(2-4), 424–439. doi: 10.1016/0012-821X(91)90220-C
- Lavé, J., & Avouac, J. P. (2001). Fluvial incision and tectonic uplift across the Himalayas of central Nepal. *Journal of Geophysical Research: Solid Earth*, 106(B11), 26561–26591. doi: 10.1029/2001jb000359
- Leever, K. (2007). *Foreland of the Romanian Carpathians, controls on late orogenic sedimentary basin evolution and Paratethys paleogeography* (PhD). VU University Amsterdam.
- Leever, K. A., Mațenco, L., Bertotti, G., Cloetingh, S., & Drijkoningen, G. G. (2006). Late orogenic vertical movements in the Carpathian Bend Zone - Seismic constraints on the transition zone from orogen to foredeep. *Basin Research*, 18(4), 521–545. doi: 10.1111/j.1365-2117.2006.00306.x
- Lindsay, J. B. (2016). Efficient hybrid breaching-filling sink removal methods for flow path enforcement in digital elevation models. *Hydrological Processes*, 30(6), 846–857. doi: 10.1002/hyp.10648
- Mațenco, L. (2017). Tectonics and exhumation of Romanian carpathians: Inferences from kinematic and thermochronological studies. In M. Rădoane & A. Vespremeanu-Stroe (Eds.), *Springer geography* (pp. 15–56). Cham: Springer International Publishing. doi: 10.1007/978-3-319-32589-7_2
- Mațenco, L., Andriessen, P., Andriessen, P., Avram, C., Bada, G., Beekman, F., ... Wong,

- H. (2013). Quantifying the mass transfer from mountain ranges to deposition in sedimentary basins: Source to sink studies in the danube basin-black sea system. *Global and Planetary Change*, 103(1), 1–18. doi: 10.1016/j.gloplacha.2013.01.003
- Mațenco, L., & Bertotti, G. (2000). Tertiary tectonic evolution of the external East Carpathians (Romania). *Tectonophysics*, 316(3-4), 255–286. doi: 10.1016/S0040-1951(99)00261-9
- Mațenco, L., Bertotti, G., Leever, K., Cloetingh, S., Schmid, S. M., Trpoanc, M., & Dinu, C. (2007). Large-scale deformation in a locked collisional boundary: Interplay between subsidence and uplift, intraplate stress, and inherited lithospheric structure in the late stage of the SE Carpathians evolution. *Tectonics*, 26(4), n/a–n/a. doi: 10.1029/2006TC001951
- Mațenco, L., Krézsek, C., Merten, S., Schmid, S., Cloetingh, S., & Andriessen, P. (2010). Characteristics of collisional orogens with low topographic build-up: An example from the Carpathians. *Terra Nova*, 22(3), 155–165. doi: 10.1111/j.1365-3121.2010.00931.x
- Mațenco, L., Munteanu, I., ter Borgh, M., Stanica, A., Tilita, M., Lericolais, G., . . . Oaie, G. (2016). The interplay between tectonics, sediment dynamics and gateways evolution in the Danube system from the Pannonian Basin to the western Black Sea. *Science of the Total Environment*, 543, 807–827. doi: 10.1016/j.scitotenv.2015.10.081
- Mandal, S. K., Lupker, M., Burg, J. P., Valla, P. G., Haghipour, N., & Christl, M. (2015). Spatial variability of ^{10}Be -derived erosion rates across the southern Peninsular Indian escarpment: A key to landscape evolution across passive margins. *Earth and Planetary Science Letters*, 425, 154–167. doi: 10.1016/j.epsl.2015.05.050
- Martin, M., & Wenzel, F. (2006). High-resolution teleseismic body wave tomography beneath SE-Romania - II. Imaging of a slab detachment scenario. *Geophysical Journal International*, 164(3), 579–595. doi: 10.1111/j.1365-246X.2006.02884.x
- Melinte-Dobrinescu, M. C., Jipa, D. C., Brustur, T., & Szobotka, S. (2008). Eastern Carpathian Cretaceous Oceanic Red Beds: Lithofacies, Biostratigraphy, and Paleoenvironment. *SEPM Special Publication*, 111–119. doi: 10.2110/sepmsp.091.111
- Merten, S., Mațenco, L., Foeken, P. T., Stuart, F. M., & Andriessen, P. A. (2010). From nappe stacking to out-of-sequence postcollisional deformations: Cretaceous to Quaternary exhumation history of the SE Carpathians assessed by low-temperature thermochronology. *Tectonics*, 29(3). doi: 10.1029/2009TC002550
- Miclăuș, C., Loiacono, F., Puglisi, D., & Baci, D. (2009). Eocene-Oligocene sedimentation in the external areas of the Moldavide Basin (Marginal Folds Nappe, Eastern Carpathians, Romania): Sedimentological, paleontological and petrographic approaches. *Geologica Carpathica*, 60(5), 397–417. doi: 10.2478/v10096-009-0029-9
- Molin, P., Fubelli, G., Nocentini, M., Sperini, S., Ignat, P., Grecu, F., & Dramis, F. (2012). Interaction of mantle dynamics, crustal tectonics, and surface processes in the topography of the Romanian Carpathians: A geomorphological approach. *Global and Planetary Change*, 90-91, 58–72. doi: 10.1016/j.gloplacha.2011.05.005
- Morisawa, M. E. (1962). Quantitative {Geomorphology} of {Some} {Watersheds} in the {Appalachian} {Plateau}. *GSA Bulletin*, 73(9), 1025–1046. doi: 10.1130/0016-7606(1962)73[1025:QGOSWI]2.0.CO;2
- Mudd, S. M. (2017). Detection of transience in eroding landscapes. *Earth Surface Processes and Landforms*, 42(1), 24–41. doi: 10.1002/esp.3923
- Mudd, S. M. (2020). Topographic data from satellites. In *In remote sensing of geomorphology; developments in earth surface processes; tarolli, p., mudd, s.m., eds* (Vol. 23, pp. 91–128). Elsevier. doi: 10.1016/B978-0-444-64177-9.00004-7
- Mudd, S. M., Attal, M., Milodowski, D. T., Grieve, S. W., & Valters, D. A. (2014). A statistical framework to quantify spatial variation in channel gradients using the integral method of channel profile analysis. *Journal of Geophysical Research: Earth Surface*, 119(2), 138–152. doi: 10.1002/2013JF002981
- Mudd, S. M., Clubb, F. J., Gailleton, B., & Hurst, M. D. (2018). How concave are river channels? *Earth Surface Dynamics*, 6(2), 505–523. doi: 10.5194/esurf-6-505-2018
- Necea, D. (2010). High-resolution morpho-tectonic profiling across an orogen: tectonic-

- controlled geomorphology and multiple dating approach in the SE Carpathians. *Tectonic-controlled geomorphology and multiple dating approach in the SE Carpathians*.
- Necea, D., Fielitz, W., Kadereit, A., Andriessen, P. A., & Dinu, C. (2013). Middle Pleistocene to Holocene fluvial terrace development and uplift-driven valley incision in the SE Carpathians, Romania. *Tectonophysics*, 602(October 2016), 332–354. doi: 10.1016/j.tecto.2013.02.039
- Necea, D., Fielitz, W., & Maţenco, L. (2005). Late Pliocene-Quaternary tectonics in the frontal part of the SE Carpathians: Insights from tectonic geomorphology. *Tectonophysics*, 410(1-4), 137–156. doi: 10.1016/j.tecto.2005.05.047
- Neely, A. B., Bookhagen, B., & Burbank, D. W. (2017). *An automated knickzone selection algorithm (KZ-Picker) to analyze transient landscapes: Calibration and validation* (Vol. 122) (No. 6). doi: 10.1002/2017JF004250
- Niemann, J. D., Gasparini, N. M., Tucker, G. E., & Bras, R. L. (2001). A quantitative evaluation of playfair’s law and its use in testing long-term stream erosion models. *Earth Surface Processes and Landforms*, 26(12), 1317–1332. doi: 10.1002/esp.272
- O’Callaghan, J. F., & Mark, D. M. (1984). The extraction of drainage networks from digital elevation data. *Computer Vision, Graphics, & Image Processing*, 28(3), 323–344. doi: 10.1016/S0734-189X(84)80011-0
- Olariu, C., Jipa, D. C., Steel, R. J., & Melinte-Dobrinescu, M. C. (2014). Genetic significance of an Albian conglomerate clastic wedge, Eastern Carpathians (Romania). *Sedimentary Geology*, 299, 42–59. doi: 10.1016/j.sedgeo.2013.10.004
- Oncescu, M. C., & Bonjer, K. P. (1997). A note on the depth recurrence and strain release of large Vrancea earthquakes. *Tectonophysics*, 272(2-4), 291–302. doi: 10.1016/S0040-1951(96)00263-6
- Ouimet, W. B., Whipple, K. X., & Granger, D. E. (2009). Beyond threshold hillslopes: Channel adjustment to base-level fall in tectonically active mountain ranges. *Geology*, 37(7), 579–582. doi: 10.1130/G30013A.1
- Penck, W. (1953). *Morphological analysis of landforms: Translation of 1924 German book by H. Czech and K.C. Boxwell*. London: Macmillan.
- Perne, M., Covington, M. D., Thaler, E. A., & Myre, J. M. (2017). Steady state, erosional continuity, and the topography of landscapes developed in layered rocks. *Earth Surface Dynamics*, 5(1), 85–100. doi: 10.5194/esurf-5-85-2017
- Perron, J. T., & Royden, L. (2013). An integral approach to bedrock river profile analysis. *Earth Surface Processes and Landforms*, 38(6), 570–576. doi: 10.1002/esp.3302
- Picotti, V., & Pazzaglia, F. J. (2008). A new active tectonic model for the construction of the Northern Apennines mountain front near Bologna (Italy). *Journal of Geophysical Research: Solid Earth*, 113(8). doi: 10.1029/2007JB005307
- Plašienka, D. (2018). Continuity and Episodicity in the Early Alpine Tectonic Evolution of the Western Carpathians: How Large-Scale Processes Are Expressed by the Orogenic Architecture and Rock Record Data. *Tectonics*, 37, 2029–2079.
- Popa, M., Radulian, M., Grecu, B., Popescu, E., & Placinta, A. O. (2005). Attenuation in Southeastern Carpathians area: Result of upper mantle inhomogeneity. *Tectonophysics*, 410(1-4), 235–249. doi: 10.1016/j.tecto.2004.12.037
- Popa, M., Radulian, M., Panaiotu, C., & Borleanu, F. (2008). Lithosphere-asthenosphere interaction at the Southeastern Carpathian Arc bend: Implications for anisotropy. *Tectonophysics*, 462(1-4), 83–88. doi: 10.1016/j.tecto.2008.03.017
- Radulian, M., Vaccari, F., Măndrescu, N., Panza, G. F., & Moldoveanu, C. L. (2000). Seismic hazard of Romania: Deterministic approach. In *Pure and applied geophysics* (Vol. 157, pp. 221–247). Springer. doi: 10.1007/pl00001096
- Roban, R. D., Krézsek, C., & Melinte-Dobrinescu, M. C. (2017). Cretaceous sedimentation in the outer Eastern Carpathians: Implications for the facies model reconstruction of the Moldavide Basin. *Sedimentary Geology*, 354, 24–42. doi: 10.1016/j.sedgeo.2017.04.001
- Royden, L., & Perron, J. T. (2013). Solutions of the stream power equation and application to the evolution of river longitudinal profiles. *Journal of Geophysical Research: Earth*

- Surface*, 118(2), 497–518. doi: 10.1002/jgrf.20031
- Royden, L. H., Clark, M. K., & Whipple, K. X. (2000). Evolution of river elevation profiles by bedrock incision; analytical solutions for transient river profiles related to changing uplift and precipitation rates. In *Eos, transactions, american geophysical union* (Vol. 81, pp. 1–2). Fall Meeting Supplement.
- Rădoane, M., Cristea, I., Dumitriu, D., & Peroiu, I. (2017). Geomorphological evolution and longitudinal profiles. In *Springer geography* (pp. 427–442). Springer. doi: 10.1007/978-3-319-32589-7_18
- Rădoane, M., Rădoane, N., & Dumitriu, D. (2003). Geomorphological evolution of longitudinal river profiles in the Carpathians. *Geomorphology*, 50(4), 293–306. doi: 10.1016/S0169-555X(02)00194-0
- Russo, R. M., Mocanu, V., Radulian, M., Popa, M., & Bonjer, K. P. (2005). Seismic attenuation in the Carpathian bend zone and surroundings. *Earth and Planetary Science Letters*, 237(3–4), 695–709. doi: 10.1016/j.epsl.2005.06.046
- Sanders, C. A. E., Andriessen, P. A. M., & Cloetingh, S. A. P. L. (1999). Life cycle of the East Carpathian orogen: Erosion history of a doubly vergent critical wedge assessed by fission track thermochronology. *Journal of Geophysical Research: Solid Earth*, 104(B12), 29095–29112. doi: 10.1029/1998jb900046
- Scherler, D., Bookhagen, B., & Strecker, M. R. (2014). Tectonic control on ^{10}Be -derived erosion rates in the Garhwal Himalaya, India. *Journal of Geophysical Research: Earth Surface*, 119(2), 83–105. doi: 10.1002/2013JF002955
- Schmid, S. M., Bernoulli, D., Fügenschuh, B., Maţenco, L., Schefer, S., Schuster, R., ... Ustaszewski, K. (2008). The Alpine-Carpathian-Dinaridic orogenic system: Correlation and evolution of tectonic units. *Swiss Journal of Geosciences*, 101(1), 139–183. doi: 10.1007/s00015-008-1247-3
- Schmid, S. M., Fügenschuh, B., Kounov, A., Maţenco, L., Nievergelt, P., Oberhänsli, R., ... van Hinsbergen, D. (2019). Tectonic units of the Alpine collision zone between Eastern Alps and western Turkey. *Gondwana Research*. doi: 10.1016/j.gr.2019.07.005
- Schmitt, G., Nuckelt, A., Knöpfler, A., & Marcu, C. (2007). Three dimensional plate kinematics in Romania. In *International symposium on strong vrancea earthquakes and risk mitigation*. Bucharest, Romania.
- Schoenbohm, L. M., Whipple, K. X., Burchfiel, B. C., & Chen, L. (2004). Geomorphic constraints on surface uplift, exhumation, and plateau growth in the Red River region, Yunnan Province, China. *Bulletin of the Geological Society of America*, 116(7–8), 895–909. doi: 10.1130/B25364.1
- Schwanghart, W., & Scherler, D. (2017). Bumps in river profiles: Uncertainty assessment and smoothing using quantile regression techniques. *Earth Surface Dynamics*, 5(4), 821–839. doi: 10.5194/esurf-5-821-2017
- Seagren, E. G., & Schoenbohm, L. M. (2019). Base Level and Lithologic Control of Drainage Reorganization in the Sierra de las Planchadas, NW Argentina. *Journal of Geophysical Research: Earth Surface*, 124, 1516–1539. doi: 10.1029/2018JF004885
- Sinclair, H. (2012). Thrust Wedge/Foreland Basin Systems. *Tectonics of Sedimentary Basins: Recent Advances*, 522–537. doi: 10.1002/9781444347166.ch26
- Steer, P., Croissant, T., Baynes, E., & Lague, D. (2019). Statistical modelling of co-seismic knickpoint formation and river response to fault slip. *Earth Surface Dynamics*, 7(3), 681–706. doi: 10.5194/esurf-7-681-2019
- Stoica, M., Lazr, I., Krijgsman, W., Vasiliev, I., Jipa, D., & Floroiu, A. (2013). Paleoenvironmental evolution of the East Carpathian foredeep during the late Miocene-early Pliocene (Dacian Basin; Romania). *Global and Planetary Change*, 103(1), 135–148. doi: 10.1016/j.gloplacha.2012.04.004
- Strong, C. M., Attal, M., Mudd, S. M., & Sinclair, H. D. (2019). Lithological control on the geomorphic evolution of the Shillong Plateau in Northeast India. *Geomorphology*, 330, 133–150. doi: 10.1016/j.geomorph.2019.01.016
- Săndulescu, M. (1984). *Geotectonica României*. Tehnica, Bucharest.

- Săndulescu, M. (1988). Cenozoic Tectonic History of the Carpathians. *The Pannonian Basin: A Study in Basin Evolution*(45), 17–25.
- Săndulescu, M., Ștefănescu, M., Butac, A., Patruș, I., & Zaharescu, P. (1981). *Genetical and structural relations between flysch and molasse (The East Carpathians)* (Tech. Rep.). Carp.-Balc. Assoc., XII Congr.
- Săndulescu, M., Krautner, H., Balintoni, I., Russo-Săndulescu, D., & Micu, M. (1981). *The structure of the East Carpathians (Moldavia-Maramures area)* (Tech. Rep.). Carp.-Balc. Assoc., XII Congr.
- Tadono, T., Nagai, H., Ishida, H., Oda, F., Naito, S., Minakawa, K., & Iwamoto, H. (2016). Generation of the 30 M-MESH global digital surface model by alos prism. *International Archives of the Photogrammetry, Remote Sensing and Spatial Information Sciences - ISPRS Archives*, 41, 157–162. doi: 10.5194/isprsarchives-XLI-B4-157-2016
- Tapponnier, P., & Molnar, P. (1977). Active faulting and tectonics in China. *Journal of Geophysical Research*, 82(20), 2905–2930. doi: 10.1029/jb082i020p02905
- ter Borgh, M. M. (2013). *Connections between sedimentary basins during continental collision : how tectonic, surface and sedimentary processes shaped the Paratethys* (PhD). Utrecht University.
- Thaler, E. A., & Covington, M. D. (2016). The influence of sandstone caprock material on bedrock channel steepness within a tectonically passive setting: Buffalo National River Basin, Arkansas, USA. *Journal of Geophysical Research: Earth Surface*, 121(9), 1635–1650. doi: 10.1002/2015JF003771
- Tărăpoancă, M., Bertotti, G., Maenco, L., Dinu, C., & Cloetingh, S. A. P. L. (2003). Architecture of the Focani Depression: A 13 km deep basin in the Carpathians bend zone (Romania). *Tectonics*, 22(6), n/a–n/a. doi: 10.1029/2002tc001486
- Tucker, G. E., & Slingerland, R. (1996). Predicting sediment flux from fold and thrust belts. *Basin Research*, 8(3), 329–349. doi: 10.1046/j.1365-2117.1996.00238.x
- Tucker, G. E., & van der Beek, P. (2013). A model for post-orogenic development of a mountain range and its foreland. *Basin Research*, 25(3), 241–259. doi: 10.1111/j.1365-2117.2012.00559.x
- van der Hoeven, A. A., Mocanu, V., Spakman, W., Nutto, M., Nuckelt, A., Maenco, L., ... Ambrosius, B. A. (2005). Observation of present-day tectonic motions in the Southeastern Carpathians: Results of the ISES/CRC-461 GPS measurements. *Earth and Planetary Science Letters*, 239(3-4), 177–184. doi: 10.1016/j.epsl.2005.09.018
- Vasiliev, I., Krijgsman, W., Langereis, C., Panaiotu, C. E., Senco, L. M., & Bertotti, G. (2004). Towards an astrochronological framework for the eastern Paratethys Mio-Pliocene sedimentary sequences of the Focsani basin (Romania). *Earth and Planetary Science Letters*, 227, 231–247. doi: 10.1016/j.epsl.2004.09.012
- Wang, Y., Zhang, H., Zheng, D., Yu, J., Pang, J., & Ma, Y. (2017). Coupling slope-area analysis, integral approach and statistic tests to steady-state bedrock river profile analysis. *Earth Surface Dynamics*, 5(1), 145–160. doi: 10.5194/esurf-5-145-2017
- Whipple, K. X. (2009). Erratum: The influence of climate on the tectonic evolution of mountain belts (Nature Geoscience 2, 97104 (2009)). *Nature Geoscience*, 2(10), 730. doi: 10.1038/ngeo638
- Willett, S. D. (1999). Orogeny and orography: The effects of erosion on the structure of mountain belts. *Journal of Geophysical Research: Solid Earth*, 104(B12), 28957–28981. doi: 10.1029/1999jb900248
- Willett, S. D., & Brandon, M. T. (2002). On steady states in mountain belts. *Geology*, 30(2), 175–178. doi: 10.1130/0091-7613(2002)030<0175:OSSIMB>2.0.CO;2
- Willett, S. D., McCoy, S. W., Taylor Perron, J., Goren, L., & Chen, C. Y. (2014). Dynamic reorganization of River Basins. *Science*, 343(6175), 1248765. doi: 10.1126/science.1248765
- Wobus, C., Whipple, K. X., Kirby, E., Snyder, N., Johnson, J., Spyropolou, K., ... Sheehan, D. (2006). Tectonics from topography: Procedures, promise, and pitfalls. *Special Paper of the Geological Society of America*, 398(04), 55–74. doi: 10.1130/2006.2398(04)

- 1016 Wobus, C. W., Crosby, B. T., & Whipple, K. X. (2006). Hanging valleys in fluvial systems:
1017 Controls on occurrence and implications for landscape evolution. *Journal of Geophysical*
1018 *Research: Earth Surface*, 111(2). doi: 10.1029/2005JF000406
- 1019 Wobus, C. W., Whipple, K. X., & Hodges, K. V. (2006). Neotectonics of the central Nepalese
1020 Himalaya: Constraints from geomorphology, detrital $^{40}\text{Ar}/^{39}\text{Ar}$ thermochronology, and
1021 thermal modeling. *Tectonics*, 25(4). doi: 10.1029/2005TC001935
- 1022 Yanites, B. J., Becker, J. K., Madritsch, H., Schnellmann, M., & Ehlers, T. A. (2017).
1023 Lithologic Effects on Landscape Response to Base Level Changes: A Modeling Study in
1024 the Context of the Eastern Jura Mountains, Switzerland. *Journal of Geophysical Research:*
1025 *Earth Surface*, 122(11), 2196–2222. doi: 10.1002/2016JF004101
- 1026 Zielke, O., Arrowsmith, J. R., Ludwig, L. G., & Akçiz, S. O. (2010). Slip in the 1857 and
1027 earlier large earthquakes along the Carrizo Plain, San Andreas Fault. *Science*, 327(5969),
1028 1119–1122. doi: 10.1126/science.1182781